© 2020. Published by The Company of Biologists Ltd | Development (2020) 147, dev181834. doi:10.1242/dev.181834

RESEARCH ARTICLE

Unique and non-redundant function of *csf1r* paralogues in regulation and evolution of post-embryonic development of the zebrafish

Joana Caetano-Lopes[1,2], Katrin Henke[1,2], Katia Urso[3,4], Jeffrey Duryea[5], Julia F. Charles[3,4], Matthew L. Warman[1,2] and Matthew P. Harris[1,2,*]

ABSTRACT

Evolution is replete with reuse of genes in different contexts, leading to multifunctional roles of signaling factors during development. Here, we explore osteoclast regulation during skeletal development through analysis of colony-stimulating factor 1 receptor (*csf1r*) function in the zebrafish. A primary role of Csf1r signaling is to regulate the proliferation, differentiation and function of myelomonocytic cells, including osteoclasts. We demonstrate the retention of two functional paralogues of *csf1r* in zebrafish. Mutant analysis indicates that the paralogues have shared, non-redundant roles in regulating osteoclast activity during the formation of the adult skeleton. *csf1ra*, however, has adopted unique roles in pigment cell patterning not seen in the second paralogue. We identify a unique noncoding element within *csf1ra* of fishes that is sufficient for controlling gene expression in pigment cells during development. As a role for Csf1r signaling in pigmentation is not observed in mammals or birds, it is likely that the overlapping roles of the two paralogues released functional constraints on *csf1ra*, allowing the signaling capacity of Csf1r to serve a novel function in the evolution of pigment pattern in fishes.

KEY WORDS: Zebrafish, *csf1r*, Osteoclast, Bone, Pigment, Evolution

INTRODUCTION

Paralogous genes, or cases of close gene copies due to duplication, represent a unique case in which to study changes in gene function throughout evolution (Ohno, 1970). Related genes, arisen from a whole-genome duplication, or ohnologues, are often lost due to drift unless these genes evolve new functions (neo-functionalization) or, alternatively, partition previously performed roles (sub-functionalization) (Kassahn et al., 2009). Instances of gene duplication can relax constraint on individual gene function and allow compartmentalization as well as evolution of novel functions. However, overlap in function of retained genes can also lead to a bias in the expression of phenotypic variability due to buffering/redundancy and inter-dependent phenotypes. It is unclear how such dependent mechanisms shape the phenotypic response of organisms and contribute to diversification in development and evolution.

Ray-finned fishes represent the most specious lineage of vertebrates, harboring great diversity in skeletal shape, size and function. Resorption of bone during skeletal development as well as homeostasis is an essential aspect to the formation of shape, structure and function of the skeleton. The form of bones of all vertebrates arises through the interactions between two main cell types: osteoblasts, which lay down new bone, and osteoclasts, which serve to remove bone (Apschner et al., 2011; Weigele and Franz-Odendaal, 2016). The role of osteoclasts in bone remodeling is quite complex, depending on the local cellular environment as well as mechanical forces on the tissue. These interactions are not yet well defined, but it is clear that they are important in the response and adaptability of the skeleton, including the dentition, to functional demands. Osteoclast differentiation and function are dependent on signaling through colony-stimulating factor1 (*csf1*) (Felix et al., 1990; Hakeda et al., 1998; Mellis et al., 2011) and its receptor, colony-stimulating factor 1 receptor (*csf1r*), a receptor tyrosine kinase expressed by cells of the monocyte/macrophage lineage and necessary for their differentiation and function (Barreda et al., 2004; Chitu and Stanley, 2017; Dai et al., 2002; Herbomel et al., 2001; Oosterhof et al., 2018; Ryan et al., 2001). In addition, in teleost fishes, *csf1ra* has been found to be expressed in neural crest progenitors and to act to regulate pigmentation cell differentiation and pattern (Parichy et al., 2000), a trait not related with Csf1 signaling in other vertebrates. It has been argued that selection on pigmentation phenotypes in fishes have contributed to their diversification (Irion et al., 2016; Salis et al., 2019). However, the additional role of *csf1r* function in regulating skeletal development may constrain the phenotypic spectrum of morphological variation in evolution.

Teleost fishes, which include the zebrafish, share an evolutionary whole-genome duplication event. Whereas previous analyses of *csf1r* gene evolution in marine fishes have uncovered two *csf1r* paralogues in many lineages (Braasch et al., 2006), in zebrafish or carp, members of a common teleost lineage Ostariophysi, a functional second paralogue could not be identified. Rather, phylogenetic analysis supported the loss of this paralogue due to drift (Braasch et al., 2006). Recently, a homologue of *csf1ra*, *csf1rb*, was identified in zebrafish regulating microglia density and distribution (Oosterhof et al., 2018). This *csf1r* paralogue showed an additive effect in the regulation of microglial density, suggesting a shared role in microglial regulation (Oosterhof et al., 2018). It remains unclear whether both genes are functionally redundant or whether a sub-functionalization occurred as effects in other tissues were not analyzed.

Here, we describe phylogenetic and functional evidence for retention of a functional *csf1rb* paralogue in zebrafish that has

[1]Orthopaedic Research Laboratories, Boston Children's Hospital, Boston, MA 02115, USA. [2]Department of Genetics, Harvard Medical School, Boston, MA 02115, USA. [3]Departments of Orthopaedics and Medicine, Brigham and Women's Hospital, Boston, MA 02115, USA. [4]Harvard Medical School, Boston, MA 02115, USA. [5]Department of Radiology, Brigham and Women's Hospital, Boston, MA 02115, USA.

*Author for correspondence (harris@genetics.med.harvard.edu)

K.U., 0000-0003-0141-4056; M.P.H., 0000-0002-7201-4693

Received 21 June 2019; Accepted 19 December 2019

Development (2020) 147, dev181834. doi:10.1242/dev.181834

overlapping and non-overlapping roles with *csf1ra* in skeletal remodeling. However, *csf1ra* has adopted a unique role in regulating pigmentation not seen in the retained paralogue. The functional buffering provided by the two paralogues may have provided context for the development of a novel function of *csf1ra* in development and important in the evolution of diversity.

RESULTS

Recent work established a potential paralogue of *csf1r* that is maintained in zebrafish (Oosterhof et al., 2018). In order to understand patterns of *csf1r* gene evolution, we assessed the phylogenetic relationship of the existing, annotated *csf1r* orthologues in vertebrates (Fig. S1). The '*b*' orthologues did not strongly differentiate as a single clade (>70 bootstrap probability). However, following Braasch et al. (2006), analysis of synteny among *csf1r* in the genomes of teleost fishes supports the conclusions that the '*b*' orthologues share a common genomic structure on the chromosome and are differentiated from '*a*' orthologues (specifically loss of *hmgxb3* and retention of *camk2a*). We further assessed clustering of the putative *csf1rb* paralogue with closely related Kit and Pdgf genes from zebrafish. An unrooted maximum likelihood tree shows strong support for the newly identified *csf1r* paralogue, *csf1rb*, as being in the *csf1r* gene family (Fig. S2A).

csf1r paralogues are differentially regulated during early development

To assess potential different roles of *csf1r* paralogues in development, we analyzed expression of both *csf1ra* and *csf1rb* during early development and in scales of the adult zebrafish. Consistent with what has been previously reported for *csf1ra* (Herbomel et al., 2001; Parichy et al., 2000; Thisse et al., 2008), we detected expression in migrating neural crest (dorsal) and in early macrophages at 2 dpf (arrowheads and arrows, Fig. 1A). We saw no *csf1rb* expression in either neural crest or early macrophages. Rather, *csf1rb* is expressed in the developing heart at 2 dpf (Fig. 1B).

We engineered a transgenic line to label mature osteoclasts that drives the expression of *DsRed* under the control of the medaka cathepsin K promoter to visualize osteoclast presence and behavior in zebrafish, (Fig. S3A). This promoter was previously defined as being specific for osteoclasts in medaka and zebrafish (Chatani et al., 2011; To et al., 2012). The *cathepsin K* (*ctsk*) transgenic line (*Tg[ctsk:DsRed]*) labeled cells in developing bones in areas where bone remodeling normally occurs (Fig. 1C; Fig. S3B-D). Importantly, *DsRed* expression colocalized with TRAP staining in scales, consistent with the *ctsk* transgenic line labeling active mature osteoclasts (Fig. S3D). As detection of *csf1r* paralogues in many tissues was difficult to achieve using standard *in situ* methods, we capitalized on the specificity of this line to experimentally isolate osteoclast cell populations using fluorescence-activated cell sorting (FACS) to assess expression of *csf1r* paralogues in skeletal cells (Fig. S4B). As a comparison, we used a second transgenic line *Tg[sp7:EGFP]* (DeLaurier et al., 2010) to isolate pre-osteoblasts from comparable tissue sources (Fig. S4A). We confirmed isolation of osteoclasts and osteoblasts through analysis of the expression of known differentiation markers for these cell populations (Fig. 1D; Fig. S4C). Consistent with the known role of Csf1r in osteoclast maturation (e.g. Chitu and Stanley, 2017), we were able to detect expression of both *csf1ra* and *csf1rb* in mature osteoclasts isolated from adult zebrafish (Fig. 1D). This expression was specific to osteoclasts, as $sp7^{+}$ osteoblasts showed no expression of either *csf1r* paralogue. After this, we isolated RNA from individual skeletal elements (fin, teeth and vertebra) with detectable populations of *Tg[ctsk:DsRed]*-positive cells and we were able to determine that both *csf1r* paralogues were expressed in these tissues (Fig. 1E), complementing the detection of osteoclasts associating with the skeletal structures.

Isolation of *csf1ra* and *csf1rb* zebrafish mutants

To test function of Csf1r receptors in zebrafish, we isolated mutants in both *csf1r* paralogues. In a mutagenesis screen, we isolated a mutant allele of *csf1ra* through expression of its recessive

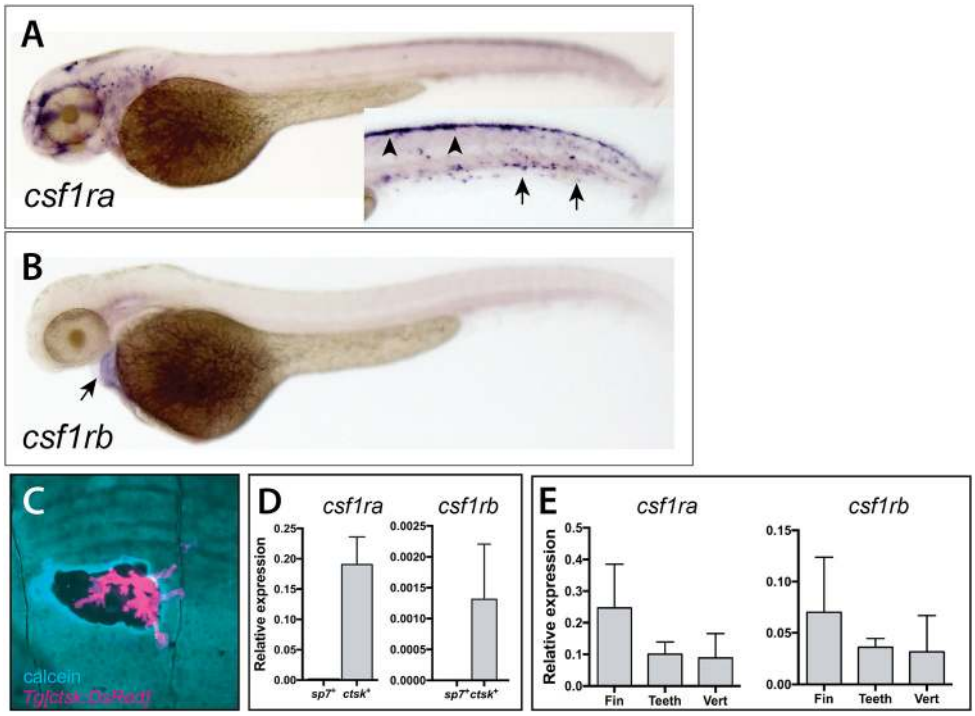

Fig. 1. Divergent expression of *csf1ra* and *csf1rb* during zebrafish early development and in scales of the adult zebrafish. Whole-mount *in situ* hybridization of *csf1ra* (A) and *csf1rb* (B). (A) *csf1ra* is expressed in cells of the pigment and hematopoietic lineages at 2 dpf; inset shows the trunk in different focal plane with pigment cells precursors (arrowheads) and hematopoietic cells (arrows). (B) In contrast, *csf1rb* is expressed at only low levels in the heart (arrow) at 2 dpf. (C) Expression of *Tg[cstk:DsRed]* in osteoclasts localizes at areas of remodeling, as shown by increased calcein staining (blue) at the periphery of the remodeled pit. (D,E) Analysis of expression of *csf1r* paralogues in isolated cells and from adult skeletal tissues. (D) Expression of *csfr1a* and *csf1rb* in isolated adult osteoblasts ($sp7^{+}$ cells) and osteoclasts ($ctsk^{+}$ cells) from wild-type zebrafish. (E) Detection of both paralogues in isolated tissues [fin, teeth and vertebra (vert)].

Development (2020) 147, dev181834. doi:10.1242/dev.181834

phenotype of altered adult pigmentation (Henke et al., 2017) (Fig. 2B). The loss of xanthophores and reduction of melanophores seen in *mh5* mirrors the phenotype previously observed in the *panther* and *salz und pfeffer* mutants due to loss of function of *csf1ra* (Parichy et al., 2000). Sequencing of the coding region of *csf1ra* in the *mh5* mutant revealed a G to T substitution at bp 1466, predicted to cause early truncation of the protein at position 454 (E454X; Fig. S2B). The mutation is tightly linked to the pigmentation phenotype and has not been observed in wild-type zebrafish populations. Given the phenotypic similarity to known alleles of *csf1ra*, and the severity of the predicted change, the G to T substitution is thought to be the causative mutation underlying the mutant phenotype.

Second, we used CRISPR/Cas9 genome editing to generate loss-of-function alleles of *csf1rb*. We induced small INDELs at the *csf1rb* locus by targeting exon 3 of the *csf1rb* gene with a pool of 5 guide RNAs. We isolated two mutant zebrafish lines, *csf1rb*^{mh108} and *csf1rb*^{mh112}. *csf1rb*^{mh108} leads to an induced frame shift in exon 3 (c.479-482delinsTGAATTAT) predicted to cause an early truncation of the protein. The *csf1rb*^{mh112} deletion is also predicted to lead to early truncation (c.476-488del; Fig. S2C). In contrast to the *csf1ra* mutants, which are easily identifiable by their aberrant pigmentation, homozygous *csf1rb* mutants do not show a detectable morphological phenotype as adults (Fig. 2C). Double *csf1ra;csf1rb* mutants exhibit a pigmentation phenotype indistinguishable from the *csf1ra* single mutants (Fig. 2D).

To determine the effect of these mutations on Csf1r activity, the expression of *csf1ra* (Fig. 2E) and *csf1rb* (Fig. 2F) was analyzed by qRT-PCR on scales of mutants and wild-type siblings. In each c*sf1ra* or *csf1rb* single mutant, we were unable to detect significant expression of the affected gene; thus, it is likely that both mutants represent null alleles. It is unlikely that the effect on expression is solely due to reduction in the number of osteoclasts, as both *csf1ra* and *csf1rb* are seen expressed in the mutant of the other paralogue. *csf1rb* expression is significantly reduced in *csf1ra* mutants, however, suggesting that the loss of *csf1ra* may limit the population of cells normally expressing *csf1rb* or, alternatively, that signaling through *csf1ra* is necessary to maintain *csf1rb* expression. In *csf1ra;csf1rb* double mutants, there was no detectable expression of either gene (Fig. 2E,F).

csf1r paralogues and remodeling of the post-embryonic zebrafish skeleton

Maturation and remodeling of the zebrafish skeleton occurs during juvenile development and throughout adulthood. Zebrafish have both mononucleated and multinucleated osteoclasts that participate in normal bone remodeling (Witten et al., 2001; Witten and Huysseune, 2009). Mononucleated osteoclasts are numerous and participate in laminar bone resorption without the presence of lacunar pits, whereas multinucleated osteoclasts are large and fewer in number but have more differentiated resorption pits. We confirmed the broad spectrum of nucleation in zebrafish osteoclasts in adult tissue. Hoechst staining of isolated *ctsk*$^{+}$ cells in adult zebrafish skeletal tissue demonstrated the recovery of a wide diversity of single and multinucleated cells (Fig. S4E,F). The presence and activity of both populations of cells in tissues *in situ* can be detected through analysis of the activity of tartrate-resistant acid phosphatase (TRAP) using histochemical methods. We addressed the role of each *csf1r* paralogue in regulating the number and function of osteoclasts in late development.

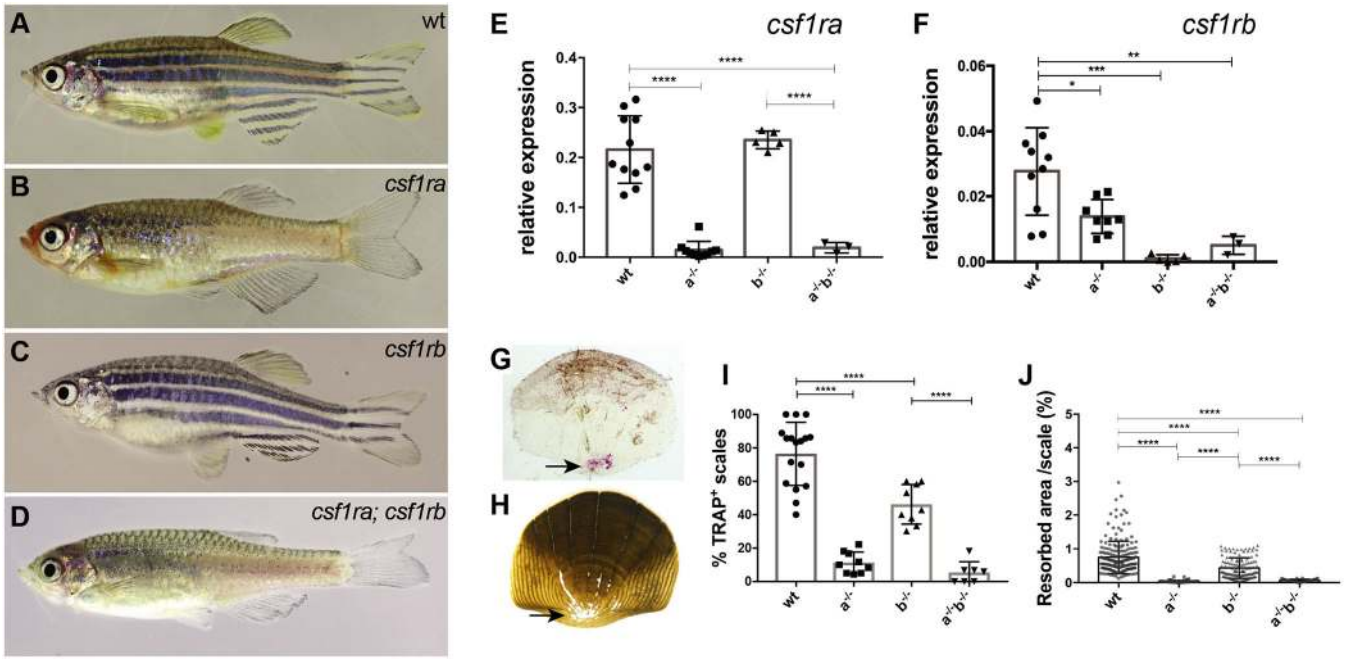

Fig. 2. Adult phenotypes of *csf1ra* and *csf1rb* mutants. (A-D) Representative photomicrographs of adult (A) wild-type zebrafish (wt), (B) homozygous *csf1ra*^{mh5}, (C) *csf1rb*^{mh108} and (D) *csf1ra*^{mh5}*;csf1rb*^{mh112} mutant zebrafish. (E,F) Quantitative RT-PCR of *csf1ra* and *csf1rb* in isolated scales of wild type, or mutants singly homozygous for *csf1ra* ($a^{-/-}$) or *csf1rb* ($b^{-/-}$), and of double mutants ($a^{-/-}b^{-/-}$). (G,H) Representative photomicrographs of scales collected from 10 wpf wild-type fish stained using TRAP (G, arrow) and (H) modified Von Kossa staining (arrow). (I,J) Quantitation of TRAP and Von Kossa staining in wild-type and mutant scales. For TRAP activity, each data point represents the percentage of scales stained by TRAP obtained by evaluating 10 scales per fish. For Von Kossa analysis, each data point represents the percentage of resorbed area per individual scale. Data are mean±s.d. **P*<0.05, ***P*<0.01, ****P*<0.001, *****P*<0.0001.

Development (2020) 147, dev181834. doi:10.1242/dev.181834

We took advantage of the dynamic homeostasis of scale mineralization in fish to assess osteoclast activity (de Vrieze et al., 2014). The scales that form across the flank of a fish are uniquely suited for analysis of matrix resorption and provide individual test cases for osteoclast function. As an indirect measure of the presence as well as the localization of osteoclasts, we performed an enzymatic assay for TRAP on scales from *csf1ra* and *csf1rb* mutants, *csf1ra;csf1rb* double mutants, and their respective wild-type siblings (Fig. 2G,I). On average, 75% of scales from wild-type fish had TRAP staining, with localized areas of staining flanking the center and in broad rings at the more distal aspect of the scale (Fig. 2G). In contrast, in homozygous *csf1ra* mutant fish, on average ∼10% of scales have TRAP staining, suggesting that some osteoclasts can still be generated in the absence of *csf1ra* (Fig. 2I). TRAP staining was not drastically affected in scales from c*sf1rb* mutants (∼50%); however, double mutants show little TRAP activity (<5% Fig. 2I). Scales containing lateral line canals were not selected, as these have been shown to have high levels of reworking and osteoclast numbers (Wada et al., 2014).

As osteoclasts function to resorb mineralized tissue, we quantified matrix resorption in fish scales by staining mineralized tissue with von Kossa staining and measuring the area of unstained material at the focus of the scale (Fig. 2H). Unstained pits or tracks in the scale, which correspond to common sites of TRAP staining in wild-type fish, are assumed to represent sites of osteoclast activity (de Vrieze et al., 2014). Evidence of resorption was detected in 99.7% of wild-type scales [coefficient of variation (CV) 5.5%]. Relative to each scale's overall size, an average of 1.2% of the area was resorbed in wild-type scales (Fig. 2J). Using this method, we detected significantly reduced resorption in *csf1ra* and *csf1ra;csf1rb* double mutant scales to less than 0.2%; *csf1rb* mutants also showed a significant, but more subtle, decrease in reworking (Fig. 2J).

csf1r paralogues differentially affect form of the vertebral skeleton

Previous work on *csf1ra*-deficient mutant zebrafish noted alterations in the formation of the neural and hemal arches in adult vertebrae (Charles et al., 2017; Chatani et al., 2011). The analysis of osteoclast distribution with our *Tg[ctsk:DsRed]* transgenic line shows localization of mature, resorbing osteoclasts to the forming vertebral neural and hemal arches (Fig. S5). Isolated vertebrae indicate that both *csf1r* paralogues are expressed in these structures (Fig. 1D,E). The proportion of *DsRed*-expressing cells in *csf1ra* mutant vertebrae was reduced in contrast to the *csf1rb* mutant vertebrae which still retained wild-type levels of *ctsk*+ cells. This is easiest seen in juveniles (2 weeks post-fertilization, Fig. S5A-C), however in 4-month-old individuals the number of osteoclasts on the formed centra and arches was extremely variable (Fig. S5D-F). This is consistent with what has been found in *Csf1r* knock-out mice, where residual macrophage populations were found, indicating that other growth factors can partially compensate for loss of *Csf1r* (Dai et al., 2002).

Using microcomputed tomography (μCT), we quantified metrics of vertebral shape and bone density in adult mutant fish (Charles et al., 2017) (Fig. 3). As shown previously (Charles et al., 2017; Chatani et al., 2011), *csf1ra* mutants show an observable alteration in the shape of the vertebrae and the pitch of the arches (Fig. 3B). In contrast, *csf1rb* mutants show vertebrae and arches that are morphologically similar to those of wild-type siblings (Fig. 3A, C). Further analysis showed that the angles of the arches in *csf1rb* mutants were significantly increased (Fig. 3J). In contrast, the arch angles in *csf1ra* and double mutant fish were decreased. Although arch angle and area of the arches are not completely independent measures, the area of arches remains unaffected in either single mutant (Fig. 3H, red, K). However, the combined action of *csf1ra* and *csf1rb* has a significant effect on the arch area, suggesting synergistic effects of deficiencies of *csf1r* paralogues on this

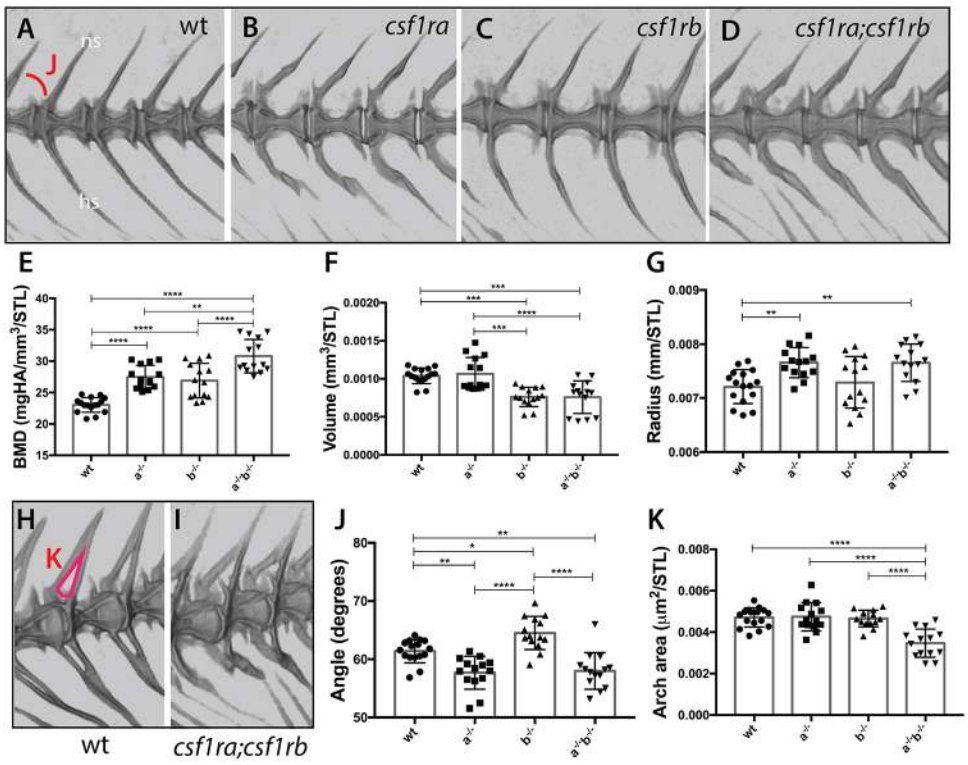

Fig. 3. Loss of *csf1r* paralogue function leads to unique and shared phenotypes in the skeleton. MicroCT imaging and quantification of skeletal metrics of the spine of age-matched *csf1r* mutants and wild-type adult siblings. (A-D) MicroCT renderings of the lateral aspect of the spine showing overall morphology and integration of serial vertebrae. The neural spines (ns) and hemal spines (hs) are indicated. The measure used for the quantification of angle of the arch (J) is noted in A. (E-G,J,K) Quantification of vertebral shape and density in *csf1r* single and double mutants: (E) bone mineral density (BMD), (F) bone volume, (G) vertebral radius, (J) angle and (K) area of the neural arch. All measurements, with the exception of angle, were standardized to standard length (STL). (H,I) visualization of neural arch area in wild-type (H) and *csf1ra*; *csf1rb* mutant (I) zebrafish; measured area used for quantification of the arch area (K) is indicated in red in H. Data are mean±s.d. **P*<0.05, ***P*<0.01, ****P*<0.001, *****P*<0.0001.

Development (2020) 147, dev181834. doi:10.1242/dev.181834

phenotype (Fig. 3I,K). These data suggest that *csfr1* paralogues may have nuanced effects in regulating vertebral morphology.

Increased bone density can occur in the context of decreased osteoclastic activity. In this regard, we found that *csf1ra* and *csf1rb* deficiency leads to an increase in bone density of the vertebral centra in an apparent additive manner (Fig. 3E). In parallel, *csf1rb* deficiency results in a reduction in bone volume, not seen in *csf1ra* mutants (Fig. 3F). Furthermore, loss of *csf1ra* leads to an increase in the radius of the vertebral body, while *csf1rb* mutants are unaffected (Fig. 3G). Thus, both paralogues are required for the regulation of shape and structure of the skeleton, with shared and unique structural components that are sensitive to alterations in their function.

Synergistic effects of *csf1r* paralogues on zebrafish dentition

Teeth are a component of the vertebrate dermal skeleton. Zebrafish develop teeth in a predictable pattern along the ventral/peripheral aspect of the last ceratobranchial arch (Fig. S6A) (Huysseune and Witten, 2006). With growth, the arch increases in size and teeth are replaced as new teeth are formed in succession (Fig. S6B). In zebrafish, resorption by osteoclasts at the tooth base is necessary for tooth loss (Huysseune et al., 1998; Witten et al., 2001; Witten and Huysseune, 2009). We reasoned that the dentition might be a sensitive skeletal structure with which to assess the role of *csf1r* in osteoclastic bone remodeling.

In staining for osteoclasts present in the mature dentition of adult fish, we observed intense TRAP staining in the arch up to the base of individual teeth (Fig. S6C). The presence of osteoclasts in this region was confirmed using the *Tg[ctsk:DsRed]* transgenic line, where osteoclasts were localized to areas of high bone deposition, as shown by calcein staining (Fig. S6D-F). Despite the abundance of osteoclasts in this region and variation in numbers in single mutants (Fig. 4G-J), whole-mount skeletal staining showed little change in the number or shape of teeth in *csf1ra* or *csf1rb* single mutants (Fig. 4B,C,E). However, changes in the retention of attachment bone can be seen at the base of the forming teeth (Fig. 4B,C, arrows). Quite strikingly, *csf1ra;csf1rb* double mutants show extreme polyodontia, with up to 20 teeth on a single arch (Fig. 4D-F). The teeth within these extended dentitions remain normal in shape and pattern, forming bouquets of teeth aligned in ventral-dorsal tracts (Fig. 4F, line). Thus, these findings suggest that the normal homeostasis of the zebrafish dentition is quite sensitive to loss of *csf1r* receptor activity, showing shared function of both receptors in remodeling of bone surrounding and ankylosing to the formed teeth, having synergistic functions in regulating tooth number in mature fish.

Identification of a unique regulatory enhancer of *csf1ra* driving novel gene function

The shared activity observed in regulation of the skeleton is in contrast to the early differences in expression observed, as well as to the overall pigmentation phenotype between the mutants analyzed (Fig. 2B,C). Given the required function for *csf1ra* in osteoclast formation as well as microglia distribution (Oosterhof et al., 2018), we hypothesized that there would be a specific and evolutionary unique gain of cis-regulatory control in *csf1ra*, shared among all teleost fishes, but unique from other vertebrates (Fig. 5A). Making use of the 11-way genomic evolutionary rate profiling (GERP) track in Ensembl, we identified a 51 bp conserved non-coding element

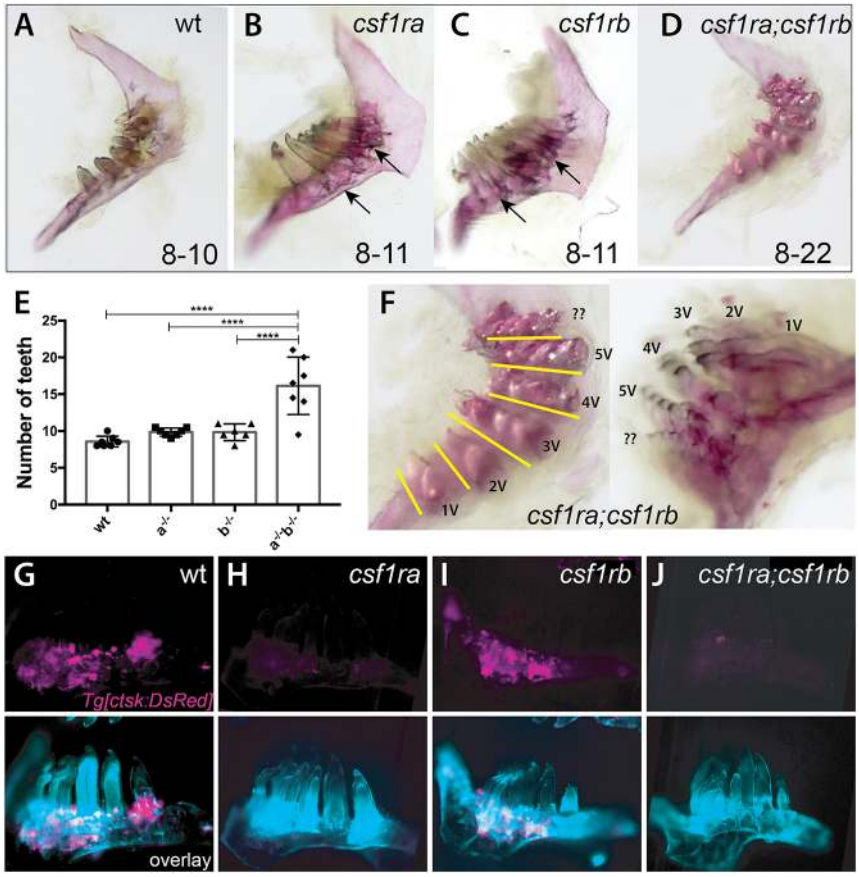

Fig. 4. *csf1r* genes show combinatorial effects in regulating patterning of the dentition and tooth number. (A-D,F) Alizarin Red stained pharyngeal arches from 4 month post-fertilization (mpf) *csf1r* mutants and wild-type siblings. Numbers on the bottom represent the range of tooth numbers on each arch (*n*=7). Arrows indicate buildup of bone surrounding base of teeth in *csf1ra* and *csf1rb* mutants (B,C). (E) Quantification of the number of teeth represented in *csf1r* mutants, double mutants and wild-type siblings (****P<0.0001). (F) Higher magnification images of dentitions from *csf1ra*;*csf1rb* double mutants showing organization of supernumerary teeth into distinct tracts (yellow line) associated with a row of normal tooth germ patterning in wild-type dentitions (Fig. S6).
(G-J) Localization of *ctsk*-positive cells (magenta) on the dentary of zebrafish *csf1r* mutants. Bottom, overlay with calcein stain (cyan).

Development (2020) 147, dev181834. doi:10.1242/dev.181834

(CNE) within *csf1ra* that is not seen in *csf1rb* (Fig. 5B; Fig. S7). We did not find evidence of this sequence in human or other amniote genomes, suggesting it is unique to teleosts (Fig. 5B); this is consistent with a gain of regulation in *csf1ra* (neo-functionalization, Fig. 5A). The identified CNE is conserved throughout evolution of teleost fishes with a broad order-specific region in *Danio* species flanking a highly conserved core region shared by all teleosts (Fig. 5C, Fig. S7). When the 50 bp CNE is placed upstream of an E1b minimal promoter (Fig. 5D), we find that it is sufficient to drive reporter expression within stellate pigment cells in clones of injected wild-type fish (P0; Fig. 5E) as well as in identified transgenic lines (F1, Fig. 5F,G).

DISCUSSION

Diversity in skeletal shape among vertebrates provides an opportunity to define shared and dissimilar mechanisms through which skeletal remodeling occurs. Previous genetic analyses in the zebrafish and medaka have shown an essential role for *csf1ra* in regulating osteoclast development and activity (Chatani et al., 2011; Mantoku et al., 2016). In zebrafish, however, the effect on skeletal development and remodeling was slight (Chatani et al., 2011). Such a limited skeletal phenotype raises questions about the importance of Csfr1 signaling in regulating skeletal form of the zebrafish, as well as the applicability of teleost fish as a model for studying osteoclast-mediated skeletal remodeling in mammals. Here, we identify broad retention of a second *csf1r* gene within teleost lineages. We identify mutants in both *csf1r* paralogues in the zebrafish, and define specific and shared functions of these genes in regulating post-embryonic development.

Functional analysis of a *csf1rb* paralogue and the broader role of *csf1r* function in skeletal remodeling

We confirmed the known phenotype of *csf1ra*-deficient zebrafish: having reduced numbers of osteoclasts resulting in altered vertebral arch shape and increased bone mass (Charles et al., 2017; Chatani et al., 2011). However, for the most part, the skeletal shape does not seem overly affected in this mutant in comparison with the osteopetrotic phenotypes observed in rodent models of *csf1* or *csf1r* deficiencies (Cotton and Gaines, 1974; Dobbins et al., 2002; Van Wesenbeeck et al., 2002). On finding a potential *csf1rb* paralogue in zebrafish, we asked whether loss of both copies of *csf1r* could better reflect shared roles in osteoclast function in vertebrate post-embryonic development. Each paralogue has quite distinct expression patterns early in development, suggesting diversification of regulation (Fig. 1). Although we do not find evidence for *csf1rb* being expressed during early development of hematopoietic cells, functionally both paralogues are essential for osteoclast function and expression is seen in mature osteoclasts,

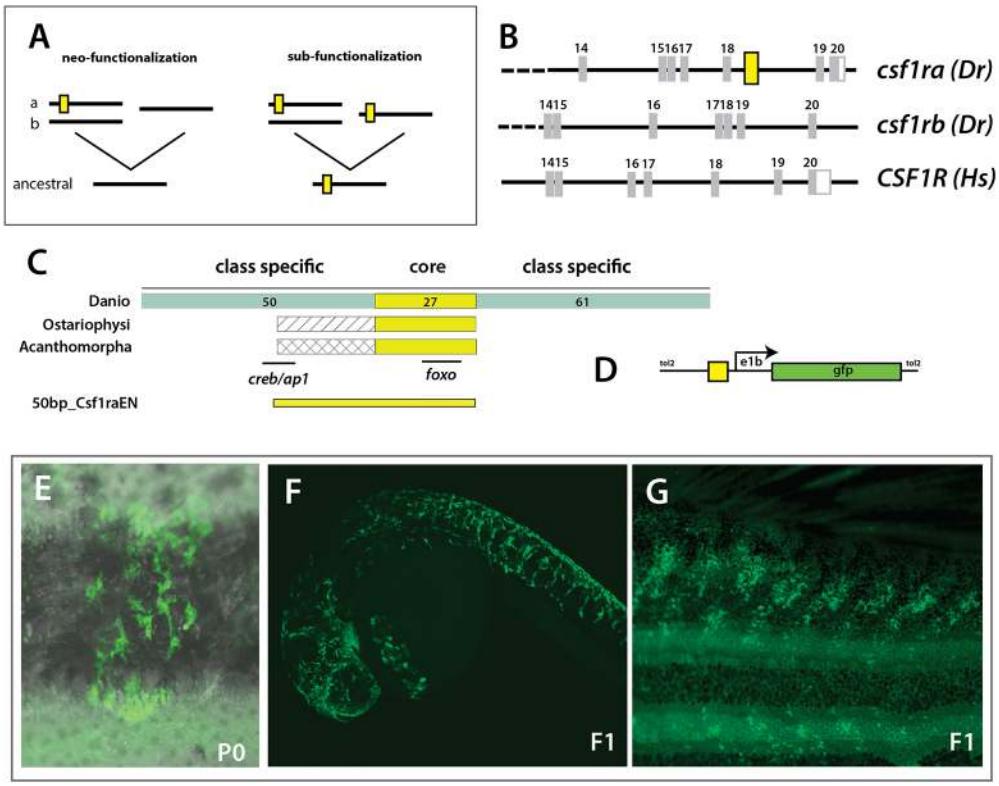

Fig. 5. Evolution of a unique enhancer controlling *csf1ra* expression in pigmentation and its variation. (A) Schematic of different mechanistic hypotheses of evolution of *csf1r* regulation. Duplication of an ancestral *csf1r* gene has led to two lineages in vertebrates within teleost fishes having two copies, '*a*' and '*b*', and tetrapods having one copy. The functional difference between '*a*' and '*b*' could be a consequence of neo-functionalization, where '*a*' gained functionality in pigment cells; or sub-functionalization, where '*a*' and '*b*' retained partial functionality of the ancestral gene; yellow box represents a hypothetical enhancer regulating expression in pigment precursors. (B) Identification of a conserved non-coding element (CNE) among fishes within *csf1ra*, not found in *csf1rb* or tetrapod *csf1r* sequences; *Dr*, *Danio rerio; Hs*, *Homo sapiens*; yellow box represents the position of the CNE. (C) Schematic and alignment of putative enhancer. Within Danios a broad 150 bp sequence is conserved with a ∼27 bp core sequence showing a 100% identity with all other teleost fishes (ostariophysans and acanthomorphs). The numbers of bp in each region are indicated. (D) Schematic of expression construct containing a 50 bp conserved region (50bp_Csf1raEN). (E-G) Representative clone of pigment cells observed in injected adult animals and in 1 dpf and adult individuals in the F1 generation; overlay of brightfield and fluorescence (E).

Development (2020) 147, dev181834. doi:10.1242/dev.181834

suggesting *csf1rb* is active in these lineages at later time points in juvenile development.

Overall, *csf1rb* shares functions with *csf1ra* in remodeling of the skeleton. Often, their activities are combinatorial with additive and synergistic effects. Patterning of the spine is particularly interesting as the effects of each paralogue can be detailed by variation in vertebrae characteristics. These phenotypes are consistent with the localization of osteoclasts on the arches during development (Fig. S5). We notice a difference in effect of *csf1ra* in maintaining resting numbers of osteoclasts compared with *csf1rb*. However, we find that the number of osteoclasts is highly variable in wild-type adults; thus, it is difficult to assign specific roles to each paralogue in terms of effect on number or localization of osteoclast populations on bone (Fig. S5). An analysis of the differential role of *csf1r* paralogues on microglia during development suggest regulation of cell migration may play a large role in the observed phenotype (Herbomel et al., 2001; Oosterhof et al., 2018); however, this is not specifically tested here. The genetic dissociation between neural arch and vertebral phenotypes has also been observed in a medaka osteopetrosis model (To et al., 2015). The modular effect of *csf1r* genes is intriguing as it would allow different regulation of these areas during development through functional variation of specific Csf1r receptors.

The essential role of osteoclasts in shaping the dentition and tooth replacement

Of the skeletal defects observed in *csf1ra;csf1rb* deficient zebrafish, the effects on tooth number are quite striking. Either *csf1ra* or *csf1rb* function is sufficient to complement the loss of the other paralogue to permit adequate removal of older teeth as new teeth are formed. The bouquet formation of the dentition in the double knockout is suggestive that osteoclasts are essential for clearance of successive teeth in a series. Similarly in medaka, a broad inhibition of osteoclast function leads to the formation of supernumerary teeth (Mantoku et al., 2016; To et al., 2015). In teleost fishes, this manifestation appears to be a failure of tooth shedding. Mice do not show tooth replacement, therefore comparable effects on dental patterning cannot be addressed. However, an important manifestation of osteoclast deficiency in mice is the failure of tooth eruption (Cotton and Gaines, 1974; Dobbins et al., 2002; Tiffee et al., 1999; Van Wesenbeeck et al., 2002). Our data detail the essential role of osteoclast function for normal tooth replacement mechanisms in the zebrafish. The synergistic effects of *csf1r* paralogue functions on the retention of teeth reveal an intricate skeletal patterning process yet to be uncovered in analyses of natural variants or in previously identified experimental mutants.

The evolution of a key role for *csf1ra* in pigment pattern diversification in teleost fishes

Teleost fishes express a broad array of pigmented varieties and pigmentation patterns are often under intense selection and are key components of fish speciation (Irion et al., 2016; Salis et al., 2019). Csf1ra function in the zebrafish was first identified through its action in regulating pigment pattern of the adult zebrafish (Haffter et al., 1996; Odenthal et al., 1996; Parichy et al., 2000). However, alteration of Csf1r activity in mammals does not lead to pigmentation defects. Whereas we find both *csf1r* paralogues are necessary for skeletal remodeling with a combined phenotype comparable with that seen in mammals, *csf1ra* has a unique role in xanthophore differentiation and stripe formation (Parichy et al., 2000). We find that *csf1rb* mutants do not show comparable pigmentation phenotypes to *csf1ra* mutants and do not show any increased effect in combination with *csf1ra* deficiency. In support of a separate role for *csf1ra* in regulating pigmentation, we find that *csf1ra* is uniquely expressed in early neural crest lineages, whereas *csf1rb* is not detected in these cells (Fig. 1). Thus, the function of *csf1ra* in neural crest differentiation and pigment pattern formation in fishes is a derived function for this gene. Concordantly, we identify a CNE within zebrafish *csf1ra* that is unique to that paralogue and highly conserved among teleosts. The CNE is not found among non-teleost vertebrates, suggesting it arose after the whole-genome duplication. The conserved CNE is sufficient to regulate expression in pigment cell during zebrafish development, suggesting this is a component of the specialization of *csf1ra*.

In diverse teleost fishes, *csf1ra* has been implicated in functional variation in pigmentation (Parichy and Johnson, 2001; Quigley et al., 2005). The pivotal role during pigment pattern formation is thought to drive diversification of the *csf1ra* gene in these groups (Salzburger et al., 2007). However, the essential role of *csf1ra* in regulating skeletogenesis would be expected to constrain the capacity of this gene in driving pigment diversity in evolution. Our finding of an essential shared role for *csf1rb* in skeletal remodeling in zebrafish suggests that sub-functionalization of *csf1r* paralogues provides buffering of function and thus the means for *csf1ra* to evolve new roles in neural crest and pigment pattern differentiation (Fig. 6), consistent with the broad retention of pigment-related gene paralogues in evolution of teleosts (Braasch

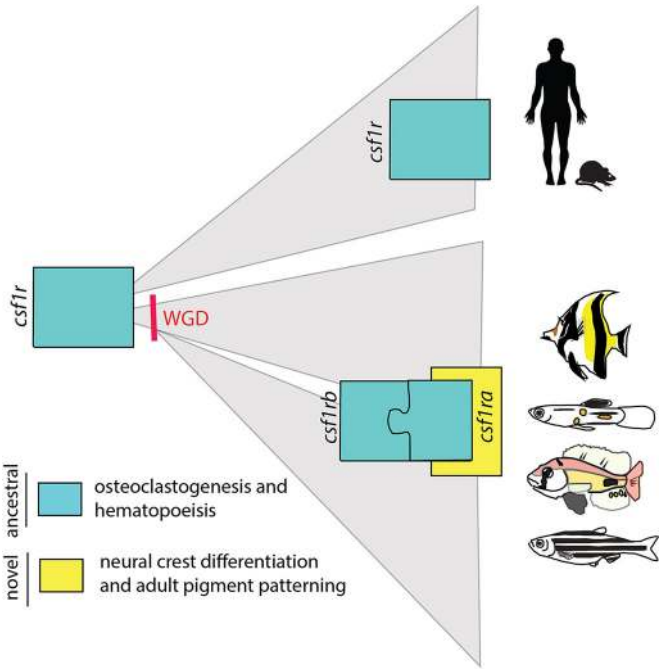

Fig. 6. Model of the evolutionary diversification of Csf1r function. Csf1r signaling is conserved in all vertebrates. CSF1R plays an important and shared role in hematopoiesis, including osteoclast differentiation. In teleost fishes, the *csf1r* locus was duplicated after the teleost-specific whole-genome duplication (WGD) event and existing paralogues are retained in most lineages. From mutational analysis, it is clear that, in teleost fish, *csf1r* genes combine to regulate osteoclast activity similar to mammals (ancestral function, blue). However, each *csf1r* paralogue has combined and singular roles in regulating remodeling. We proposed a model in which, in teleosts, *csf1ra* acquired a novel function in regulating pigment pattern specification (new function, yellow). This role would be a derived function for this gene and has led to differential selection of *csf1ra* in regulating the pigment pattern of the adult fish.

Development (2020) 147, dev181834. doi:10.1242/dev.181834

et al., 2009; Lorin et al., 2018). We provide here the first molecular and functional evidence of this neo-functionalization.

MATERIALS AND METHODS

Phylogenetic analysis

The phylogenetic relationship between zebrafish *csf1ra*, *csf1rb*, *pdgfra*, *pdgfrb*, *kita* and *kitb* was established by retrieving the amino acid sequences from NCBI (O'Leary et al., 2016) and ENSEMBL (Yates et al., 2016) databases. Protein sequences were aligned using MUSCLE (Edgar, 2004) multiple sequence alignment tool. A phylogenetic tree was constructed based on amino acid difference with the maximum likelihood algorithm in MEGA version 7.0.18 (Kumar et al., 2016). The reliability of the tree was assessed by bootstrapping, using 500 replicates, and bootstrap support ≥70 was considered significant. The resulting tree was imported to iTOL version 3.2.4 (Letunic and Bork, 2016) for final editing.

To examine the phylogenetic relationship between zebrafish *csf1ra* and *csf1rb* paralogues and their corresponding vertebrate orthologues, the amino acid sequences of *Astyanax mexicanus*, *Clupea harengus*, *Ctenopharyngodon idellus*, *Cyprinodon variegatus*, *Danio rerio*, *Esox lucius*, *Homo sapiens*, *Latimeria chalumnae*, *Mus musculus*, *Oreochromis niloticus*, *Oryzias latipes*, *Poecilia reticulata*, *Pygocentrus nattereri*, *Salmo salar*, *Sinocyclocheilus anshuiensis*, *Sinocyclocheilus grahami*, *Sinocyclocheilus rhinocerous*, *Takifugu rubripes* and *Xenopus tropicalis* were retrieved from NCBI and ENSEMBL databases. The same strategy described before was used to construct a phylogenetic tree. Accession numbers of protein sequences used in the analysis are listed in Table S1.

Zebrafish husbandry and identification of mutant lines

Zebrafish strains were maintained under standard conditions (Westerfield, 1993) in compliance with internal regulatory review at Boston Children's Hospital. At the indicated age, fish were euthanized with 20% MS-222 and scales were collected from the anterior area of either side of the trunk.

The *csf1ra*^{mh5} mutant line was isolated in the Harris lab in an ENU mutagenesis screen. The mutation in *csf1ra* was identified by a candidate gene approach due to similarity to *panther* and *salz und pfeffer* mutants. A missense mutation in *csf1ra* was detected in cDNA from homozygous 4 dpf *csf1ra*^{mh5} mutant larvae amplified using two primer combinations [*csf1ra*-f1 (ACGGTCCAGTGACGTTTCTT) with *csf1ra*-r2 (CTCTTTGCCCAGACCGTAAG); and *csf1ra*-f2 (GGCAGTGACACCTTCTCCAT) with *csf1ra*-r1 (GTCTGCAGCTGTTGTGCTGT)] to cover a large component of the *csf1ra*-coding region (NM_131672.1). For genotyping of individuals from genomic DNA, we used primers *csf1ra*_g_f1 (CGGCCTTCTGTGAATTTTGT) and *csf1ra*_g_r1 (TGCCTAATTACCCAAACTTGC). The *csf1ra* mutation is consistently linked to the pigment phenotype.

CRISPR-Cas9 technology and specific guide RNAs (gRNA) designed against *csf1rb* were used for the generation of mutants. Specifically, five gRNAs were designed using CHOPCHOP (Montague et al., 2014) (chopchop.cbu.uib.no) targeting *csf1rb* exon 3 (gRNA1-GGTCATCCCAGGAGGAACAG, gRNA2-GCAGTATAATTCATCCCAGG, gRNA3-GCCTGGGATGAATTATACTG, gRNA4-GATACTGCGGATCCCAGACG and gRNA5-GTCTGTATGGTGAACATGAG). Guide RNAs were synthesized as described by Gagnon et al. (2014). Briefly, templates for gRNA transcription were generated by annealing gene-specific oligonucleotides containing the T7 promoter sequence (5′-TAATACGACTCACTATA-3′), the target site without the protospacer adjacent motif (PAM) sequence and a complementary region to a constant oligonucleotide encoding the reverse complement of the tracrRNA tail. Guide RNAs were transcribed using the MEGAshortscript T7 kit (Ambion). *Cas9* mRNA was synthesized from a linearized pCS2-nCas9n plasmid (Jao et al., 2013) using the mMESSAGE mMACHINE SP6 kit (Ambion). To generate mutant fish, a pool of the five gRNAs (100 ng/µl) and *Cas9* mRNA (500 ng/µl) were injected into one-cell stage zebrafish AB wild-type embryos.

CRISPR-induced mutations were identified though amplification of a 743 bp genomic region containing *csf1rb* exon 3 using primers 5′-AAACAGATCCCGACAAAGCC-3′ and 5′-CGTCCGATTTTGACCGCG-3′ followed by T7 endonuclease digestion. To establish mutant lines, injected fish were grown to adulthood and outcrossed to AB wild-type fish. The nature of induced INDELs created by CRISPR/Cas9 was identified in the F1 progeny by sequencing of subcloned PCR products.

Generation of cathepsin K osteoclast reporter line

We used a 3 kb upstream region of the medaka (*Oryzias latipes*) cathepsin K gene, previously shown to drive expression in osteoclasts in zebrafish (Chatani et al., 2011), and cloned it into the p5E-MCS plasmid (228, Tol2kit; Kwan et al., 2007) in front of the *DsRed* sequence flanked by FRT sites. To enable simultaneous generation of an osteoclast reporter and an osteoclast-specific line driving *Cre* expression, sequence encoding *Cre* (from the plasmid pOG231; O'Gorman et al., 1997) was cloned in a middle entry gateway plasmid (pENTR/D-TOPO, Life Technologies). For generation of an expression reporter construct, we used the multisite Gateway system in which the 3′ entry plasmid (302, p3E-polyA) and the destination vector (395, pDestTol2CG2) were obtained from the Tol2kit (Kwan et al., 2007). As a marker for transgenesis, the pDestTol2CG2 destination vector contains a *cmlc2* promoter driving GFP expression in the heart. The construct was made via recombination from gateway-based clones using LR clonase II (Life Technologies).

To generate transgenic fish, plasmid DNA (10 ng/µl) and transposase RNA (10 ng/µl) were injected into one-cell stage zebrafish embryos. These animals were raised to adulthood and outcrossed to Tuebingen (Tue) wild-type fish. Progeny were screened for cardiac GFP expression at 48 hpf and raised to establish the *Tg[Ola.ctsk:FRT-DsRed-STOP-FRT,Cre, cmlc2:GFP]* transgenic line (referred to here as *Tg[ctsk:DsRed]*). *Tg[ctsk:DsRed]* transgenic fish were crossed with *csf1ra*^{mh5} and *csf1rb*^{mh108} to visualize the cathepsin K-expressing cells in mutant lines. Progeny were stained overnight with 100 µg/l calcein (Sigma) solution in water as counterstain for mineralized matrix.

In situ hybridization

csf1ra and *csf1rb in situ* hybridization was performed in scales using a modified version of the Thisse et al. protocol (Thisse and Thisse, 2008). At 24 hpf, 30 mg/l of N-Phenylthiourea (PTU, Sigma) was added to the developing embryos to prevent pigment development. For *in situ* hybridization, 700-800 bp of unique sequence for each gene were amplified from cDNA [*csf1ra*, (f) ACTGGACTTCCTCGCTGCTA, (r) GTCTGCAGCTGTTGTGCTGT; *csf1rb*, (f) CGACCTCCTCAACTTCTTGC, (r) TCAGGTGCCTTCGAAGTTCT] and used to transcribe sense and antisense digoxigenin (DIG)-labeled riboprobes with DIG RNA labeling kit SP6/T7 (Roche). Probes were hybridized at 60°C against 24, 48 and 96 hpf wild-type larva and in adult scales, and the hybridization was visualized using nitro blue tetrazolium/5-bromo-4-chloro-3-indolyl-phosphate (NBT/BCIP) staining.

Cell isolation and sorting

The transgenic lines *Tg[ctsk:DsRed]* and *Tg[sp7:EGFP]* (DeLaurier et al., 2010) were used to isolate osteoclasts and osteoblasts, respectively. Protocol was based on methodologies outlined by Madel et al. (2018) and Buettner et al. (2015). Fish were euthanized and tissue samples harvested for isolation of cells. Tissues were digested by vigorous shaking at 30°C in dissociation solution [0.21% trypsin-EDTA (Invitrogen), 16 mg/ml collagenase from *Clostridium histolyticum*, type IA (Sigma)] for 15 min. The cell suspension was washed with Dulbecco's Modified Eagle Media (DMEM) supplemented with 10% of fetal bovine serum (FBS, Invitrogen) and filtered on a 40 µm nylon mesh. The filtered cell suspension was layered on Histopaque-1077 (Sigma) at a 2:1 ratio and centrifuged at 400 ***g***, without acceleration or break, for 30 min in a swinging bucket rotor. Both the ring and the pellet were collected in PBS+2%FBS. Immediately prior to sorting, cells were stained with 1X SYTOX Blue (Invitrogen). After doublet exclusion, live cells were identified by the absence of SYTOX Blue staining. *EGFP* or *DsRed*-positive cells were separated on an FACSAria II cell sorter (BD Biosciences) using an 85 µm nozzle at a flow rate of ∼2000 events/s. For RNA studies, sorted cells were collected directly in RNA lysis buffer for subsequent RNA extraction.

For analysis of DNA content, after isolation cells were counted and stained using Hoechst 33342 (Sigma) 10 µg/ml per 10^6 cells per 500 µl at 37°C for 30 min (method adapted from Madel et al., 2018; Schmid and

Development (2020) 147, dev181834. doi:10.1242/dev.181834

Sakamoto, 2001). Cells were washed in PBS+2% FBS prior to FACS analysis. After removal of doublets, *DsRed*$^{+}$ or *EGFP*$^{+}$ cells we identified and analyzed according to Hoechst 33342 expression. A Hoechst 33342 histogram was plotted and *sp7:EGFP*$^{+}$ cells were used to determine gating strategy for mononuclear cells.

RNA isolation and quantitative RT-PCR

Scales from adult fish were collected in Trizol reagent (Life Technology), the tissue was mechanically homogenized and RNA was extracted using the Direct-zol RNA kit (Zymo Research). Sorted cells were collected directly in RNeasy plus micro kit (Qiagen) lysis buffer and RNA was extracted according to the manufacturer's recommendation.

Reverse transcription was performed with the Protoscript first strand cDNA synthesis kit (New England Biolabs). Quantitative real-time PCR (qRT-PCR) was performed using Sybr green reagent (Life Technologies) in duplicate. Expression levels were normalized to tubulin. RT-PCR primers used in the analysis are: *csf1ra* (f) AATCAGAACCACCTGTCCCG; *csf1ra* (r) CGACCAGGTTAAAGGCCACA; *csf1rb* (f) TAAAAGGCAATGCACGGCTG, *csf1rb* (r) CGCAAAATCTGGTTGTGGCA; *ctsk* (f) CGCCTTCAGATACGTCAGCA, *ctsk* (r) GGTCAGTGCCCTCTCGTTAC; *sp7* (f) TCGATTCTGGAGGAGGAAACAC, *sp7* (r) CGTCCGTTTTTAGCGCTCTG; tubulin (f) GTACGTGGGTGAGGGTATGG, tubulin (r) ACACAGCAGGCAGCATTTCTA.

Tartrate resistant acid phosphatase staining

Tartrate resistant acid phosphatase (TRAP) staining solution was made from equal volumes of solution A and solution B. Solution A contained naphtol AS-MX phosphate (100 µg/ml), N,N-dimethylformamide (1% v/v) in acetate buffer (0.1 M); solution B contained Fast Red LB Violet Salt (600 µg/ml) in acetate buffer (0.1 M). After mixing solutions A and B, sodium tartrate (50 mM) was added and the pH adjusted to 5.0. The solution was then filtered to remove large particles.

Freshly collected scales from 10 weeks post-fertilization (wpf) fish were washed in PBS and fixed in 4% paraformaldehyde at room temperature for 1 min. Samples were washed twice with distilled H_2O and stained with pre-warmed TRAP staining solution at 37°C for 15 min. The number of scales with TRAP staining was counted and calculated as percentage of total scales (minimum of 10 scales per fish, 10 fish per group was used).

Staining of bone mineralized matrix

Whole-mount silver nitrate staining was defined after a modified von Kossa staining method (de Vrieze et al., 2014). Scales from 10 wpf fish were stained immediately after collection with freshly prepared silver nitrate (2.5% $AgNO_3$ in distilled H_2O, Sigma) for 30 min at room temperature. Scales were washed in distilled H_2O before being observed under a microscope. Analysis of the resorbed area was performed by applying a threshold to the image in Image J (Schneider et al., 2012). At least ten fish per group, with ten scales per fish were used for each experiment.

Teeth from adult (4mpf) *csf1ra*^{mh5}, *csf1rb*^{mh108}, *csf1ra*^{mh5};*csf1rb*^{mh112} and wild-type siblings were stained overnight in an 100 µg/ml Alizarin Red solution (Sigma) and destained in 0.5% KOH solution.

Micro-computed tomography

Adult (4 mpf) *csf1ra*^{mh5}, *csf1rb*^{mh108}, *csf1ra*^{mh5};*csf1rb*^{mh112} and wild-type siblings were euthanized and fixed in 10% formalin for 24 h and kept in 70% ethanol. Caudal vertebrae and teeth were imaged using micro-computed tomography (µCT) with a voxel size of 6 µm, using an X-ray tube potential of 55 kVp, an X-ray intensity of 0.145 mA and an integration time of 600 ms (Scanco µCT35). Vertebral analysis was performed using custom software to determine neural arch area and angle, vertebral volume, radius, and bone mineral density, as performed previously (Charles et al., 2017). Two sets of three seed points were placed manually on the anterior and posterior faces of the vertebral body. The radius was determined from fitting each set to a circle and calculating the average. The length was defined as the distance between the centers of the fitted circles. The volume was total number of voxels defined as bone by the thresholding algorithm and the angle was measured between the ray connecting the averaged circumference and a second line defined by seed points placed on the arch. With the exception of the angle, all parameters were normalized with the standard length (STL) of each fish. Thresholding was performed equally through all samples. Analysis of variant measures at different thresholds showed comparable data between wild-type and mutant fish. 3D reconstruction was made in Amira 6.0 (FEI) software.

Generation of *csf1ra*-CNE overexpression reporter lines

Using the 11-way genomic evolutionary rate profiling (GERP) track in ENSEMBL, we identified a conserved non-coding element (CNE) within *csf1ra*. To examine sequence similarities between Danios, *Gadus morhua*, *Takifugu rubripes*, *Tetraodon nigroviridis*, *Oreochromis niloticus*, *Gasterosteus aculeatus*, *Oryzias latipes*, *Poecilia formosa*, *Xiphophorus maculatus* and *Astyanax mexicanus*, genomic *csf1ra* sequences were retrieved from NCBI (O'Leary et al., 2016) and ENSEMBL (Yates et al., 2016) databases. CNE sequences were aligned using Clustal Omega multiple sequence alignment tool (Madeira et al., 2019). TFbind was used for transcription factors binding site prediction (Tsunoda and Takagi, 1999). Accession numbers of genomic DNA sequences used in the analysis are listed in Table S2.

Enhancer sequences (50 bp) from *D. rerio* were cloned into the E1b-GFP-Tol2 plasmid upstream of the E1b minimal promoter (Birnbaum et al., 2012). To generate transgenic fish, plasmid DNA (10 ng/µl) and transposase RNA (10 ng/µl) were injected into one-cell stage Tue wild-type zebrafish embryos. These animals were raised to adulthood and outcrossed to Tue wild-type fish. Progeny were screened for GFP expression at 24 hpf and raised to establish the transgenic line.

Statistical analysis

Statistical analysis was performed using SPSS Statistics 23.0 (IBM). Continuous variables were expressed as mean±s.d. Groups were compared using analysis of variance (ANOVA) test followed by Bonferroni's multiple comparison test. Statistical significance was set at $P<0.05$.

Acknowledgements

The authors thank Mrs. Althea James for assistance in zebrafish husbandry, the Flow Cytometry Research Facility at Boston Children's Hospital, and David Parichy in sharing unpublished whole genome data from select *Danio* species.

Competing interests

The authors declare no competing or financial interests.

Author contributions

Conceptualization: J.C.-L., K.H., K.U., J.F.C., M.P.H.; Methodology: J.C.-L., K.H., J.D., J.F.C., M.P.H.; Validation: J.C.-L., K.H., J.F.C., M.P.H.; Formal analysis: J.C.-L., K.H., K.U., J.D., J.F.C., M.P.H.; Investigation: J.C.-L., K.H., K.U., J.D., J.F.C., M.P.H.; Resources: M.L.W., M.P.H.; Data curation: J.C.-L., K.H., J.D., J.F.C., M.P.H.; Writing - original draft: M.P.H.; Writing - review & editing: J.C.-L., K.H., K.U., J.F.C., M.L.W., M.P.H.; Visualization: J.C.-L., K.H., J.D., J.F.C., M.P.H.; Supervision: J.F.C., M.L.W., M.P.H.; Project administration: J.F.C., M.L.W., M.P.H.; Funding acquisition: J.F.C., M.L.W., M.P.H.

Funding

This work was partially supported by the National Institutes of Health (U01 DE024434 to M.P.H., K08 AR062590 to J.F.C. and GM122471 to D.P.). Deposited in PMC for release after 12 months.

Supplementary information

Supplementary information available online at http://dev.biologists.org/lookup/doi/10.1242/dev.181834.supplemental

References

Apschner, A., Schulte-Merker, S. and Witten, P. E. (2011). Not all bones are created equal - using zebrafish and other teleost species in osteogenesis research. *Methods Cell Biol.* **105**, 239-255. doi:10.1016/B978-0-12-381320-6.00010-2

Barreda, D. R., Hanington, P. C. and Belosevic, M. (2004). Regulation of myeloid development and function by colony stimulating factors. *Dev. Comp. Immunol.* **28**, 509-554. doi:10.1016/j.dci.2003.09.010

Birnbaum, R. Y., Clowney, E. J., Agamy, O., Kim, M. J., Zhao, J., Yamanaka, T., Pappalardo, Z., Clarke, S. L., Wenger, A. M., Nguyen, L. et al. (2012). Coding exons function as tissue-specific enhancers of nearby genes. *Genome Res.* **22**, 1059-1068. doi:10.1101/gr.133546.111

Braasch, I., Salzburger, W. and Meyer, A. (2006). Asymmetric evolution in two fish-specifically duplicated receptor tyrosine kinase paralogons involved in teleost coloration. *Mol. Biol. Evol.* **23**, 1192-1202. doi:10.1093/molbev/msk003

Braasch, I., Brunet, F., Volff, J.-N. and Schartl, M. (2009). Pigmentation pathway evolution after whole-genome duplication in fish. *Genome Biol. Evol.* **1**, 479-493. doi:10.1093/gbe/evp050

Buettner, A., Sundaram, S., Vyas, H., Yu, T., Mathavan, S. and Winkler, C. (2015). Fluorescence-activated cell sorting (FACS) of osteoblasts and osteoclasts for RNA sequencing in a medaka, Oryzias latipes (Temming & Schlegel, 1846), osteoporosis model. *J. Appl. Ichthyol.* **34**, 481-488. doi:10.1111/jai.13660

Charles, J. F., Sury, M., Tsang, K., Urso, K., Henke, K., Huang, Y., Russell, R., Duryea, J. and Harris, M. P. (2017). Utility of quantitative micro-computed tomographic analysis in zebrafish to define gene function during skeletogenesis. *Bone* **101**, 162-171. doi:10.1016/j.bone.2017.05.001

Chatani, M., Takano, Y. and Kudo, A. (2011). Osteoclasts in bone modeling, as revealed by in vivo imaging, are essential for organogenesis in fish. *Dev. Biol.* **360**, 96-109. doi:10.1016/j.ydbio.2011.09.013

Chitu, V. and Stanley, E. R. (2017). Regulation of embryonic and postnatal development by the CSF-1 receptor. *Curr. Top. Dev. Biol.* **123**, 229-275. doi:10.1016/bs.ctdb.2016.10.004

Cotton, W. R. and Gaines, J. F. (1974). Unerupted dentition secondary to congenital osteopetrosis in the Osborne-Mendel rat. *Proc. Soc. Exp. Biol. Med.* **146**, 554-561. doi:10.3181/00379727-146-38146

Dai, X.-M., Ryan, G. R., Hapel, A. J., Dominguez, M. G., Russell, R. G., Kapp, S., Sylvestre, V. and Stanley, E. R. (2002). Targeted disruption of the mouse colony-stimulating factor 1 receptor gene results in osteopetrosis, mononuclear phagocyte deficiency, increased primitive progenitor cell frequencies, and reproductive defects. *Blood* **99**, 111-120. doi:10.1182/blood.V99.1.111

de Vrieze, E., Moren, M., Metz, J. R., Flik, G. and Lie, K. K. (2014). Arachidonic acid enhances turnover of the dermal skeleton: studies on zebrafish scales. *PLoS ONE* **9**, e89347. doi:10.1371/journal.pone.0089347

DeLaurier, A., Eames, B. F., Blanco-Sánchez, B., Peng, G., He, X., Swartz, M. E., Ullmann, B., Westerfield, M. and Kimmel, C. B. (2010). Zebrafish sp7:EGFP: a transgenic for studying otic vesicle formation, skeletogenesis, and bone regeneration. *Genesis* **48**, 505-511. doi:10.1002/dvg.20639

Dobbins, D. E., Sood, R., Hashiramoto, A., Hansen, C. T., Wilder, R. L. and Remmers, E. F. (2002). Mutation of macrophage colony stimulating factor (Csf1) causes osteopetrosis in the tl rat. *Biochem. Biophys. Res. Commun.* **294**, 1114-1120. doi:10.1016/S0006-291X(02)00598-3

Edgar, R. C. (2004). MUSCLE: multiple sequence alignment with high accuracy and high throughput. *Nucleic Acids Res.* **32**, 1792-1797. doi:10.1093/nar/gkh340

Felix, R., Cecchini, M. G. and Fleisch, H. (1990). Macrophage colony stimulating factor restores in vivo bone resorption in the op/op osteopetrotic mouse. *Endocrinology* **127**, 2592-2594. doi:10.1210/endo-127-5-2592

Gagnon, J. A., Valen, E., Thyme, S. B., Huang, P., Ahkmetova, L., Pauli, A., Montague, T. G., Zimmerman, S., Richter, C. and Schier, A. F. (2014). Efficient mutagenesis by Cas9 protein-mediated oligonucleotide insertion and large-scale assessment of single-guide RNAs. *PLoS ONE* **9**, e98186. doi:10.1371/journal.pone.0098186

Haffter, P., Odenthal, J., Mullins, M. C., Lin, S., Farrell, M. J., Vogelsang, E., Haas, F., Brand, M., van Eeden, F. J. M., Furutani-Seiki, M. et al. (1996). Mutations affecting pigmentation and shape of the adult zebrafish. *Dev. Genes Evol.* **206**, 260-276. doi:10.1007/s004270050051

Hakeda, Y., Kobayashi, Y., Yamaguchi, K., Yasuda, H., Tsuda, E., Higashio, K., Miyata, T. and Kumegawa, M. (1998). Osteoclastogenesis inhibitory factor (OCIF) directly inhibits bone-resorbing activity of isolated mature osteoclasts. *Biochem. Biophys. Res. Commun.* **251**, 796-801. doi:10.1006/bbrc.1998.9523

Henke, K., Daane, J. M., Hawkins, M. B., Dooley, C. M., Busch-Nentwich, E. M., Stemple, D. L. and Harris, M. P. (2017). Genetic screen for postembryonic development in the zebrafish (Danio rerio): dominant mutations affecting adult form. *Genetics* **207**, 609-623. doi:10.1534/genetics.117.300187

Herbomel, P., Thisse, B. and Thisse, C. (2001). Zebrafish early macrophages colonize cephalic mesenchyme and developing brain, retina, and epidermis through a M-CSF receptor-dependent invasive process. *Dev. Biol.* **238**, 274-288. doi:10.1006/dbio.2001.0393

Huysseune, A. and Witten, P. E. (2006). Developmental mechanisms underlying tooth patterning in continuously replacing osteichthyan dentitions. *J. Exp. Zool. B Mol. Dev. Evol.* **306**, 204-215. doi:10.1002/jez.b.21091

Huysseune, A., Van der heyden, C. and Sire, J.-Y. (1998). Early development of the zebrafish (Danio rerio) pharyngeal dentition (Teleostei, Cyprinidae). *Anat. Embryol.* **198**, 289-305. doi:10.1007/s004290050185

Irion, U., Singh, A. P. and Nüsslein-Volhard, C. (2016). The developmental genetics of vertebrate color pattern formation: lessons from zebrafish. *Curr. Top. Dev. Biol.* **117**, 141-169. doi:10.1016/bs.ctdb.2015.12.012

Jao, L.-E., Wente, S. R. and Chen, W. (2013). Efficient multiplex biallelic zebrafish genome editing using a CRISPR nuclease system. *Proc. Natl. Acad. Sci. USA* **110**, 13904-13909. doi:10.1073/pnas.1308335110

Kassahn, K. S., Dang, V. T., Wilkins, S. J., Perkins, A. C. and Ragan, M. A. (2009). Evolution of gene function and regulatory control after whole-genome duplication: comparative analyses in vertebrates. *Genome Res.* **19**, 1404-1418. doi:10.1101/gr.086827.108

Kumar, S., Stecher, G. and Tamura, K. (2016). MEGA7: molecular evolutionary genetics analysis version 7.0 for bigger datasets. *Mol. Biol. Evol.* **33**, 1870-1874. doi:10.1093/molbev/msw054

Kwan, K. M., Fujimoto, E., Grabher, C., Mangum, B. D., Hardy, M. E., Campbell, D. S., Parant, J. M., Yost, H. J., Kanki, J. P. and Chien, C.-B. (2007). The Tol2kit: a multisite gateway-based construction kit for Tol2 transposon transgenesis constructs. *Dev. Dyn.* **236**, 3088-3099. doi:10.1002/dvdy.21343

Letunic, I. and Bork, P. (2016). Interactive tree of life (iTOL) v3: an online tool for the display and annotation of phylogenetic and other trees. *Nucleic Acids Res.* **44**, W242-W245. doi:10.1093/nar/gkw290

Lorin, T., Brunet, F. G., Laudet, V. and Volff, J.-N. (2018). Teleost fish-specific preferential retention of pigmentation gene-containing families after whole genome duplications in vertebrates. *G3* **8**, 1795-1806. doi:10.1534/g3.118.200201

Madeira, F., Park, Y. M., Lee, J., Buso, N., Gur, T., Madhusoodanan, N., Basutkar, P., Tivey, A. R. N., Potter, S. C., Finn, R. D. et al. (2019). The EMBL-EBI search and sequence analysis tools APIs in 2019. *Nucleic Acids Res.* **47**, W636-W641. doi:10.1093/nar/gkz268

Madel, M.-B., Ibáñez, L., Rouleau, M., Wakkach, A. and Blin-Wakkach, C. (2018). A novel reliable and efficient procedure for purification of mature osteoclasts allowing functional assays in mouse cells. *Front. Immunol.* **9**, 2567. doi:10.3389/fimmu.2018.02567

Mantoku, A., Chatani, M., Aono, K., Inohaya, K. and Kudo, A. (2016). Osteoblast and osteoclast behaviors in the turnover of attachment bones during medaka tooth replacement. *Dev. Biol.* **409**, 370-381. doi:10.1016/j.ydbio.2015.12.002

Mellis, D. J., Itzstein, C., Helfrich, M. H. and Crockett, J. C. (2011). The skeleton: a multi-functional complex organ: the role of key signalling pathways in osteoclast differentiation and in bone resorption. *J. Endocrinol.* **211**, 131-143. doi:10.1530/JOE-11-0212

Montague, T. G., Cruz, J. M., Gagnon, J. A., Church, G. M. and Valen, E. (2014). CHOPCHOP: a CRISPR/Cas9 and TALEN web tool for genome editing. *Nucleic Acids Res.* **42**, W401-W407. doi:10.1093/nar/gku410

Odenthal, J., Rossnagel, K., Haffter, P., Kelsh, R. N., Vogelsang, E., Brand, M., van Eeden, F. J., Furutani-Seiki, M., Granato, M., Hammerschmidt, M. et al. (1996). Mutations affecting xanthophore pigmentation in the zebrafish, Danio rerio. *Development* **123**, 391-398.

O'Gorman, S., Dagenais, N. A., Qian, M. and Marchuk, Y. (1997). Protamine-Cre recombinase transgenes efficiently recombine target sequences in the male germ line of mice, but not in embryonic stem cells. *Proc. Natl. Acad. Sci. USA* **94**, 14602-14607. doi:10.1073/pnas.94.26.14602

Ohno, S. (1970). *Evolution by Gene Duplication*. New York: Springer-Verlag.

O'Leary, N. A., Wright, M. W., Brister, J. R., Ciufo, S., Haddad, D., McVeigh, R., Rajput, B., Robbertse, B., Smith-White, B., Ako-Adjei, D. et al. (2016). Reference sequence (RefSeq) database at NCBI: current status, taxonomic expansion, and functional annotation. *Nucleic Acids Res.* **44**, D733-D745. doi:10.1093/nar/gkv1189

Oosterhof, N., Kuil, L. E., van der Linde, H. C., Burm, S. M., Berdowski, W., van Ijcken, W. F. J., van Swieten, J. C., Hol, E. M., Verheijen, M. H. G. and van Ham, T. J. (2018). Colony-Stimulating Factor 1 Receptor (CSF1R) regulates microglia density and distribution, but not microglia differentiation in vivo. *Cell Rep.* **24**, 1203-1217.e6. doi:10.1016/j.celrep.2018.06.113

Parichy, D. M. and Johnson, S. L. (2001). Zebrafish hybrids suggest genetic mechanisms for pigment pattern diversification in Danio. *Dev. Genes Evol.* **211**, 319-328. doi:10.1007/s004270100155

Parichy, D. M., Ransom, D. G., Paw, B., Zon, L. I. and Johnson, S. L. (2000). An orthologue of the kit-related gene fms is required for development of neural crest-derived xanthophores and a subpopulation of adult melanocytes in the zebrafish, Danio rerio. *Development* **127**, 3031-3044.

Quigley, I. K., Manuel, J. L., Roberts, R. A., Nuckels, R. J., Herrington, E. R., MacDonald, E. L. and Parichy, D. M. (2005). Evolutionary diversification of pigment pattern in Danio fishes: differential fms dependence and stripe loss in D. albolineatus. *Development* **132**, 89-104. doi:10.1242/dev.01547

Ryan, G. R., Dai, X.-M., Dominguez, M. G., Tong, W., Chuan, F., Chisholm, O., Russell, R. G., Pollard, J. W. and Stanley, E. R. (2001). Rescue of the colony-stimulating factor 1 (CSF-1)-nullizygous mouse (Csf1(op)/Csf1(op)) phenotype with a CSF-1 transgene and identification of sites of local CSF-1 synthesis. *Blood* **98**, 74-84. doi:10.1182/blood.V98.1.74

Salis, P., Lorin, T., Laudet, V. and Frédérich, B. (2019). Magic traits in magic fish: understanding color pattern evolution using reef fish. *Trends Genet.* **35**, 265-278. doi:10.1016/j.tig.2019.01.006

Salzburger, W., Braasch, I. and Meyer, A. (2007). Adaptive sequence evolution in a color gene involved in the formation of the characteristic egg-dummies of male haplochromine cichlid fishes. *BMC Biol.* **5**, 51. doi:10.1186/1741-7007-5-51

Schmid, I. and Sakamoto, K. M. (2001). Analysis of DNA content and green fluorescent protein expression. *Curr. Protoc. Cytom.* **16**, 7.16.1-7.16.10. doi:10.1002/0471142956.cy0716s16
Schneider, C. A., Rasband, W. S. and Eliceiri, K. W. (2012). NIH Image to ImageJ: 25 years of image analysis. *Nat. Methods* **9**, 671-675. doi:10.1038/nmeth.2089
Thisse, C. and Thisse, B. (2008). High-resolution in situ hybridization to whole-mount zebrafish embryos. *Nat. Protoc.* **3**, 59-69. doi:10.1038/nprot.2007.514
Thisse, B., Wright, G. J. and Thisse, C. (2008). Embryonic and larval expression patterns from a large scale screening for novel low affinity extracellular protein interactions. ZFIN Direct Data Submission. zfin.org/ZDB-PUB-080227-22
Tiffee, J. C., Xing, L., Nilsson, S. and Boyce, B. F. (1999). Dental abnormalities associated with failure of tooth eruption in src knockout and op/op mice. *Calcif. Tissue Int.* **65**, 53-58. doi:10.1007/s002239900657
To, T. T., Witten, P. E., Renn, J., Bhattacharya, D., Huysseune, A. and Winkler, C. (2012). Rankl-induced osteoclastogenesis leads to loss of mineralization in a medaka osteoporosis model. *Development* **139**, 141-150. doi:10.1242/dev.071035
To, T. T., Witten, P. E., Huysseune, A. and Winkler, C. (2015). An adult osteopetrosis model in medaka reveals the importance of osteoclast function for bone remodeling in teleost fish. *Comp. Biochem. Physiol. C Toxicol. Pharmacol.* **178**, 68-75. doi:10.1016/j.cbpc.2015.08.007
Tsunoda, T. and Takagi, T. (1999). Estimating transcription factor bindability on DNA. *Bioinformatics* **15**, 622-630. doi:10.1093/bioinformatics/15.7.622
Van Wesenbeeck, L., Odgren, P. R., MacKay, C. A., D'Angelo, M., Safadi, F. F., Popoff, S. N., Van Hul, W. and Marks, S. C.Jr. (2002). The osteopetrotic mutation toothless (tl) is a loss-of-function frameshift mutation in the rat Csf1 gene: evidence of a crucial role for CSF-1 in osteoclastogenesis and endochondral ossification. *Proc. Natl. Acad. Sci. USA* **99**, 14303-14308. doi:10.1073/pnas.202332999
Wada, H., Iwasaki, M. and Kawakami, K. (2014). Development of the lateral line canal system through a bone remodeling process in zebrafish. *Dev. Biol.* **392**, 1-14. doi:10.1016/j.ydbio.2014.05.004
Weigele, J. and Franz-Odendaal, T. A. (2016). Functional bone histology of zebrafish reveals two types of endochondral ossification, different types of osteoblast clusters and a new bone type. *J. Anat.* **229**, 92-103. doi:10.1111/joa.12480
Westerfield, M. (1993). *The Zebrafish Book; A Guide for the Laboratory Use of Zebrafish (Brachydanio rerio)*, 2nd edn.: University of Oregon Press.
Witten, P. E. and Huysseune, A. (2009). A comparative view on mechanisms and functions of skeletal remodelling in teleost fish, with special emphasis on osteoclasts and their function. *Biol. Rev. Camb. Philos. Soc.* **84**, 315-346. doi:10.1111/j.1469-185X.2009.00077.x
Witten, P. E., Hansen, A. and Hall, B. K. (2001). Features of mono- and multinucleated bone resorbing cells of the zebrafish Danio rerio and their contribution to skeletal development, remodeling, and growth. *J. Morphol.* **250**, 197-207. doi:10.1002/jmor.1065
Yates, A., Akanni, W., Amode, M. R., Barrell, D., Billis, K., Carvalho-Silva, D., Cummins, C., Clapham, P., Fitzgerald, S., Gil, L. et al. (2016). Ensembl 2016. *Nucleic Acids Res.* **44**, D710-D716. doi:10.1093/nar/gkv1157